Chemistry Associated with Hypersonic Vehicles

Thomas R. A. Bussing*
Boeing Military Airplane Company, Seattle, Washington
and
Scott Eberhardt†
University of Washington, Seattle, Washington

A series of chemical equilibrium, chemical nonequilibrium, and thermal nonequilibrium calculations are performed for various chemical processes related to a Single Stage To Orbit Hydrogen Fueled Airbreathing Hypersonic Vehicle (SSTOHFAHV). The processes include air dissociation downstream of a 60- and 30-deg oblique shock and H_2-air combustion. The calculations are applied to two typical SSTOHFAHV trajectories.

Nomenclature

a_{ik} = ith polynomial coefficient for species k
c = speed of sound
c^0_{pk} = coefficient of heat at constant pressure for species k
e_v = vibrational energy
e^*_v = equilibrium vibrational energy
G^0 = standard state Gibbs free energy
H^0_k = standard state species enthalpy
h = static enthalpy
M = Mach number
p = pressure
R = gas constant
S^0_k = standard state species entropy
T = gas temperature (translational and rotational)
T_v = vibrational temperature
u = velocity
V_n = normal velocity
γ = ratio of specific heats
ϕ = fuel equivalence ratio
ρ = density
τ = characteristic vibrational relaxation time
θ = shock angle

Subscripts

2 = conditions downstream of shock wave
k = species k
n = normal component
v = vibration
∞ = freestream condition

Introduction

THERE is a renewed national interest in hypersonics. A prime motivation for this interest is the desire to develop a Single Stage To Orbit Hydrogen Fueled Airbreathing Hypersonic Vehicle, or SSTOHFAHV. This vehicle and its derivatives have been the subject of many recent conceptual studies. A significant result of these studies is that major portions of the vehicle will have to be designed using computational tools since ground-based test facilities do not exist for all flight conditions. This conclusion marks a turning point in computational fluid dynamics (CFD) in that a vehicle will be designed and flown based primarily on numerical computations. It is therefore necessary to ensure that the CFD codes contain correct physical models for flight conditions of interest.

The first step in selecting physical models is to determine flight conditions. A recent review paper by Howe[1] discusses the aerothermal environment about generic advanced space transportation systems. Suggested are optimum ascent trajectories where an airbreathing space plane will gain its speed in the upper atmosphere. The low density of the air combined with hypervelocity speeds, with the associated high static temperatures, leads to chemical and thermal nonequilibrium in the external flowfield of the vehicle. In addition to the complex external flow, supersonic combustion has been cited as the key technology in the development of the vehicle.[2] The chemistry associated with the combustion process and the expansion in the nozzle dictates the effectiveness of the airbreathing alternative to current rocket technology. Both the external and the internal fluid mechanics of the vehicle suggest that chemical kinetics and vibrational energy must be included in CFD calculations to some extent.

Including species conservation equations and decomposing energy into its separate modes expands the complexity of current CFD codes significantly. If nonequilibrium chemical kinetics is required, a fully coupled set of conservation equations must be solved, as in Refs. 3–6. However, simplified models for chemical and vibrational processes might be available for certain conditions. For example, at the lower altitudes and velocities, one expects chemical and thermal equilibrium. In a CFD code this may be effectively modeled using NASA's RGAS tables or Tannehill's curve fits.[7] If the flow is frozen, i.e., if the chemical relaxation processes are much slower than the convection of the gas past the vehicle, ideal-gas calculations may suffice. An important step in the design program of a hypersonic vehicle is to determine what level of chemical and thermal modeling is required.

In this paper an attempt is made to characterize the chemical and thermal properties of the gases associated with an airbreathing space plane. First, the vehicle is decomposed into six regions of specific gas physics, as shown in Fig. 1. The regions are the nose, wing/tail leading edge, boundary layers, forebody/ramps/inlets, combustor/flame holder, and nozzle. The first three regions are important in determining aerodynamic characteristics and surface heating. Precise design of reusable thermal protection hinges around the ability to predict surface temperatures and chemistry. The three last regions are important in determining engine performance characteristics. They encompass engine inflow, combustion, and outflow, respectively. The ability to predict these three flows is essential to achieving accurate engine analysis. These

Received Nov. 16, 1987; revision received June 7, 1988.

*Principle Engineer. Member AIAA.
†Assistant Professor, Department of Aeronautics and Astronautics. Member AIAA.

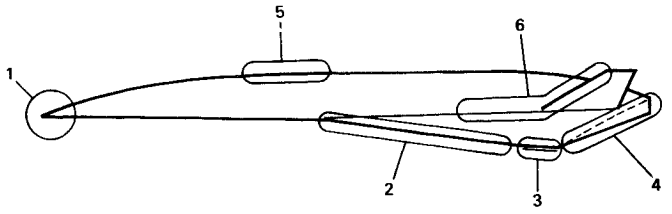

REGIONS	CHEMISTRY
1 NOSE	AIR THERMAL AND CHEMICAL NON-EQUILIBRIUM
2 RAMPS/INLETS	AIR CHEMICAL NON-EQUILIBRIUM
3 COMBUSTOR/FLAME HOLDING	H_2-AIR CHEMICAL NON-EQUILIBRIUM
4 NOZZLE	H_2-AIR CHEMICAL NON-EQUILIBRIUM
5 BOUNDARY LAYERS	AIR/H_2-AIR CHEMICAL NON-EQUILIBRIUM
6 WING/TAIL LEADING EDGE	AIR CHEMICAL NON-EQUILIBRIUM

Fig. 1 Chemistry characterization of a hypersonic vehicle (SSTO-HFAHV).

six regions encompass most of the important physics that must be studied to effectively design an airbreathing space plane.

The next step is to select general properties common to the regions listed. Two processes are selected for this study. One is the air chemistry behind a shock wave, and the other is the hydrogen-air chemistry of the engine. With these two processes, four of the six regions can be approximated. The boundary layer involves processes that depend on wall conditions and are not considered in this study. The chemistry of the ramp/inlet system is dominated by its boundary layer and, therefore, is also not considered.

To date, the model for all chemistry characterization is that of Bray,[8] where chemical relaxation lengths and compressibility are plotted against velocity for various pressures and temperatures. In this article more detailed information, such as equilibrium species concentrations and chemical and thermal relaxation lengths, is presented. However, rather than provide less information at many pressures and temperatures, detailed information is provided at specific pressures and temperatures. For the external flow calculations, these conditions are selected to correspond to points along two generic ascent trajectories. A discussion of these trajectories is provided later. For the engine and nozzle calculations, the pressures and temperatures are selected as sample combustor operating conditions.

The data presented in this format provide a convenient means of assessing the importance of chemical relaxation and specific species concentrations. By using both the equilibrium chemistry composition and the nonequilibrium length scales, one can reconstruct the chemical physics of the flow. For example, a 30-deg oblique shock wave exhibits very long length scales, suggesting nonequilibrium flow. This is a consequence of lower static temperatures and high convective velocities. However, a glance at the equilibrium values shows that limited dissociation occurs only at higher Mach numbers. Therefore, we find that, although the nonequilibrium region is long, the effects of chemical kinetics are much less important for a 30-deg oblique shock than for a 60-deg shock.

The hydrogen-air data is intended to supplement simple engine performance analysis programs. An engine designed to operate at specific temperatures and pressures will exhibit certain length scales and combustion products that may or may not be detrimental to engine performance. At high temperatures, for example, significant dissociation of the combustion products occurs. Alternatively, lower temperatures may exhibit favorable species distribution in equilibrium, but the reaction length scales may be long. The assumptions used in this study are presented in the following sections, followed by explanations of the results.

Table 1 Freestream conditions for ascent trajectories

M	h, km	p, atm	T, °K	ρ, kg/m^3	u-m/s 60 deg	u-m/s 30 deg
			Lower trajectory			
0.0	0.0	1.000	288.2	1.225		
2.5	7.6	0.372	238.8	0.502	670.7	387.3
5.0	18.3	7.06E-2	216.7	0.115	1277.8	737.8
7.5	24.4	2.72E-2	221.1	4.34E-2	1935.6	1117.5
10.0	25.9	2.16E-2	222.6	3.42E-2	2589.4	1495.0
12.5	27.4	1.75E-2	223.9	2.75E-2	3247.6	1875.0
15.0	30.5	1.10E-2	227.0	1.70E-2	3923.1	2265.0
17.5	32.0	8.77E-2	228.5	1.36E-2	4592.1	2651.3
20.0	35.1	5.60E-3	236.8	8.35E-3	5343.3	3085.0
22.5	38.1	3.65E-3	245.3	5.12E-3	6114.6	3530.3
25.0	44.2	1.57E-3	262.8	2.16E-3	7025.6	4056.3
			Upper trajectory			
0.0	0.0	1.000	288.2	1.225		
2.5	24.4	2.72E-2	221.1	4.43E-2	645.2	372.5
5.0	29.0	1.37E-2	225.5	2.15E-2	1303.4	752.5
7.5	32.0	8.77E-3	228.5	1.36E-2	1968.0	1136.3
10.0	33.5	7.00E-3	232.4	1.07E-2	2646.6	1528.0
12.5	34.0	6.55E-3	233.7	9.89E-3	3318.0	1915.6
15.0	37.0	4.28E-3	242.1	6.24E-3	4050.4	2338.5
17.5	42.7	1.91E-3	258.6	2.61E-3	4878.5	2816.6
20.0	48.8	8.72E-4	270.7	1.14E-3	5712.3	3298.0
22.5	54.9	4.10E-4	264.7	5.40E-4	6367.9	3676.5
25.0	68.6	6.82E-5	225.6	1.07E-4	6499.5	3752.5

Trajectory

The trajectory, as mentioned previously, involves acceleration in the lower-density upper atmosphere. Two generic accent trajectories, given in Ref. 9, are used in this study. The two trajectories are upper and lower bounds of the SSTO-HFAHV flight envelope, as suggested in the reference. These trajectories are not intended to be interpreted as actual accent trajectories, but are selected as bounds. These trajectories are listed in Table 1.

Trajectory points at 2.5-Mach intervals are selected as data points to study. Freestream conditions are obtained from the U.S. Standard Atmosphere.[10] The external gas dynamic calculations use this data as input.

Data plotted with Mach number on the abscissa implies trajectory conditions from Table 1. In other words, for each Mach number, there is an assumed pressure, temperature, density, etc., corresponding to the two trajectories.

Forebody and Leading Edges

The wing leading edge and nose have a finite radius and, therefore, will have a detached bow shock. The thermal and chemical environment in this shock layer is dictated by the high velocities, low densities, and small radii of the leading edges. Figure 2 shows a schematic of the nonequilibrium processes that take place in the vicinity of these regions. In particular, the figure shows that following the bow shock, the flow will be in both thermal and chemical nonequilibrium. The extent of these regions and their importance to vehicle design will be approximated with simple oblique shock models. The oblique shock models represent the flow properties of the bow/forebody shock away from the immediate vicinity of the nose. These models do not include the nonequilibrium processes along the stagnation streamline or the boundary layer near the body surface. However, the flowfield between the forebody shock and the boundary layer can be modeled effectively with this approach. Recent studies have been performed to characterize the thermodynamic heating using simple sphere and cylinder models but have not contained any

information on the nonequilibrium time scales.[11] For these regions, one-dimensional calculations are performed to study chemical relaxation lengths and equilibrium concentrations behind an oblique shock wave.

Combustor and Nozzle

There are numerous studies in progress dealing with analysis of SCRAMJET combustors, nozzles, and afterbodies. Computational analysis ranges from one-dimensional complicated chemical kinetics modeling to two- and three-dimensional simple chemical kinetics flow simulations. In these studies, as the number of dimensions increases, the complexity of the combustion models tends to decrease.

In this article, engine and nozzle performance is characterized by temperature, pressure, and fuel equivalence ratio ϕ. This characterization eliminates trajectory dependence and focuses on engine performance parameters. The engine is assumed to maintain specific temperatures and pressures at the nozzle entrance. The fuel equivalence ratio is a measure of the amount of fuel available. When $\phi = 1$, the proportions of fuel to oxygen are stoichiometric. In other words, if $\phi < 1$, all fuel should be burned. Typically, SCRAMJET engines are designed to operate at $\phi \approx 1$–5 to provide adequate vehicle cooling as well as thrust.

The important performance parameters of this article are reaction times and species concentrations at equilibrium. Reaction times are selected over reaction lengths because engine velocities can vary for a given combustor pressure and temperature. The equilibrium concentrations represent the amount of dissociation and recombination for a given temperature and pressure. The relaxation time gives a measure of how long the fluid must remain in the engine to be combusted. Note that details of supersonic mixing are not covered in this paper so nonuniformity of the engine flow must be considered in addition to the information provided here.

In the following sections we discuss in detail the assumptions made and the methods used to perform the calculations. Results are then presented to characterize the regions of interest in the manner suggested.

Chemistry Models

Equilibrium Chemistry

In this paper we have chosen to characterize the external chemistry around a hypersonic vehicle by two parameters. The first is the equilibrium chemistry composition and the second is the characteristic relaxation length, or time, for the production or destruction of a particular species. The following discussion outlines the method and assumptions used to determine the equilibrium chemistry compositions.

Equilibrium calculations are performed using a package developed at NASA Lewis by Gordon and McBride.[12] The basis of their method is that equilibrium occurs when the Gibbs free energy is minimized. Since its introduction in 1958,[13] it has seen wide use.[4–17] Results are in good agreement with equilibrium coefficient calculations and are generally reached more efficiently. In addition to Gibbs free energy minimization, elemental mass is conserved. Lagrange multipliers are used to solve the simultaneous system of equations.

The program requires an expression for the Gibbs free energy G, the enthalpy H, and the specific heat at constant pressure c_p for each species. In this study these expressions are given from the JANAF tables[19,20] and use the following polynomial fits:

$$c^0_{pk}/R = a_{1k} + a_{2k}T + a_{3k}T^2 + a_{4k}T^3 + a_{5k}T^4$$

$$\frac{H^0_k}{RT} = a_{1k} + \frac{a_{2k}}{2}T + \frac{a_{3k}}{3}T^2 + \frac{a_{4k}}{4}T^3 + \frac{a_{5k}}{5}T^4 + \frac{a_{6k}}{T}$$

$$\frac{S^0_k}{R} = a_{1k}\ell nT + a_{2k}T + \frac{a_{3k}}{2}T^2 + \frac{a_{4k}}{3}T^3 + \frac{a_{5k}}{4}T^4 + a_{7k}$$

and

$$G^0 = H^0 - TS^0$$

The coefficients a_{jk} are supplied at several temperature ranges to provide the most accurate fit. Separate tables are used for the air and hydrogen-air cases discussed in Ref. 18.

The package requires as input two state variables. The algorithm has been developed for an enthalpy, pressure (p,H) input and a pressure, temperature (p,T) input. Output from the program includes other thermodynamic properties (density, enthalpy, etc.) and species molar concentrations.

Chemical Nonequilibrium

Chemical nonequilibrium can occur in connection with a variety of processes on an SSOHAHV. The processes include

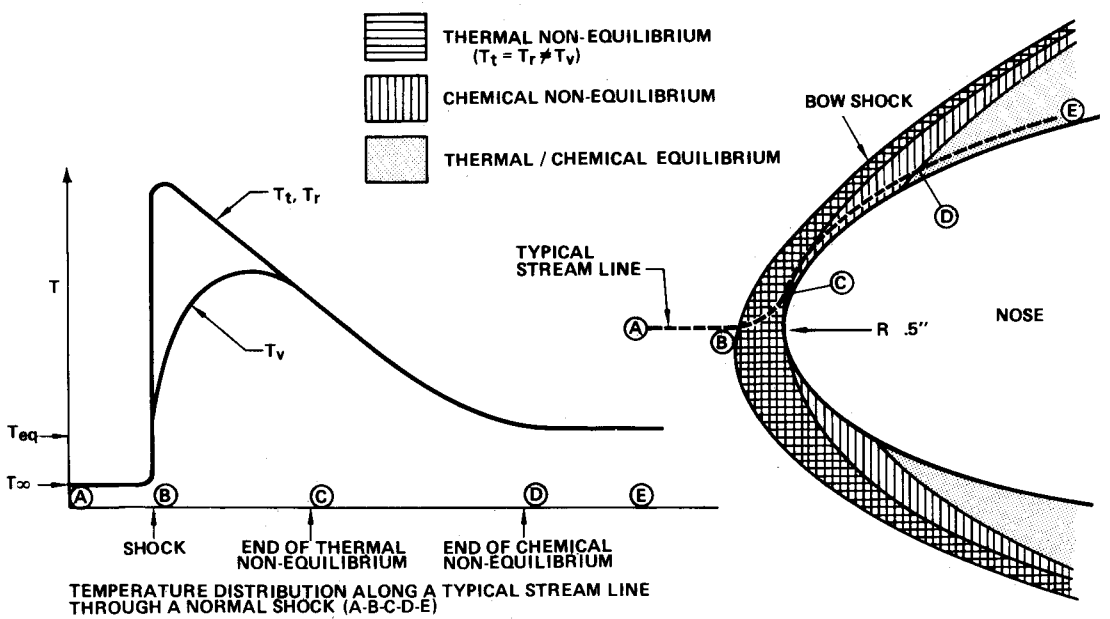

Fig. 2 Nonequilibrium physics of the nose region.

the flow downstream of a shock wave, wall surface chemistry, and combustion, to name a few. This paper investigates air chemical nonequilibrium length scales downstream of oblique shock waves and nonequilibrium H_2-air combustion time scales for typical hydrogen-fueled scramjet operating conditions.

As mentioned, two different types of calculations are performed for this article. The first involved computing the chemical nonequilibrium flowfield downstream of an oblique shock wave. The calculations are performed with the CHEMKIN nonequilibrium chemistry code described in Refs. 21 and 22. The flow downstream of a shock is assumed to be adiabatic, with transport phenomena associated with mass diffusion, thermal conduction, and viscous effects assumed to be negligible. Initial conditions for the governing equations are derived from the Rankine-Hugoniot relations for flow across a normal shock. Across the shock it is assumed that translational, rotational, and vibrational modes are in equilibrium. Thus, only chemical nonequilibrium is modeled.

It should be noted that vibrational nonequilibrium can have a profound effect on chemical nonequilibrium. For instance, most recently, Park[26] has shown with his coupled vibration-dissociation model that relaxation lengths can increase by an order of magnitude when both processes are modeled together. However, because of the complexity of coupled vibration-dissociation models, and because only order-of-magnitude estimates are of interest here, no attempt has been made to incorporate vibrational effects in these calculations.

The thermodynamic properties given by Esch[20] are used for temperatures above 6000 K. The flowfield is computed with the one-dimensional Euler equations coupled with a set of species transport equations that describe the nonequilibrium chemistry modeled in this article. The nonequilibrium length scales are defined as the distance behind the shock required for various fluid and chemical quantities to reach 95% of their respective equilibrium values. Figure 3 shows the relaxation behavior of a typical quantity, for example temperature, behind a shock. The relaxation distance D_1 is shown in Fig. 3. When oblique shocks are analyzed, the nonequilibrium length scales are determined by the following method. First the normal component of velocity is used to determine the shock jump conditions. This is followed by a nonequilibrium chemistry calculation to determine a normal length behind the shock. To find the resultant length of the nonequilibrium region, the normal length is added vectorially to the tangential length ($V_t \cdot \tau$). Additional details related to the equations and algorithm are given in Ref. 21.

The second type of calculation involves computing nonequilibrium time scales for H_2-air combustion at constant pressure. A variety of temperatures, pressures, and ϕ typical of the operating conditions in a hydrogen-fueled scramjet are considered here. A system of ordinary differential equations describing adiabatic, constant pressure chemical kinetics is used to compute the nonequilibrium time scales. The CHEMKIN chemistry package[21] is used for these calculations. The time scales computed here represent the total time to equilibrium minus the ignition time, i.e., the reaction time. Figure 4 shows the time history of a typical quantity, e.g., temperature. The total time to equilibrium is defined as the time required for a typical quantity to reach 95% of equilibrium while the ignition time is taken to be the time required for a typical quantity to go from its initial state to 1% of its final equilibrium state. The reaction time is illustrated in Fig. 4, i.e., $t_2 - t_1$. Knowing the reaction time and the local fluid velocity, one can compute the reaction length ($d = V \cdot t$). The ignition delay time is not considered here, since it is strongly dependent upon the ignition source and thus highly problem-specific. In addition, the ignition source can be adjusted to make the ignition time small compared to the reaction time. Thus, reaction time is generally considered the best quantity to measure when studying combustion time scales for constant pressure reactions.[27]

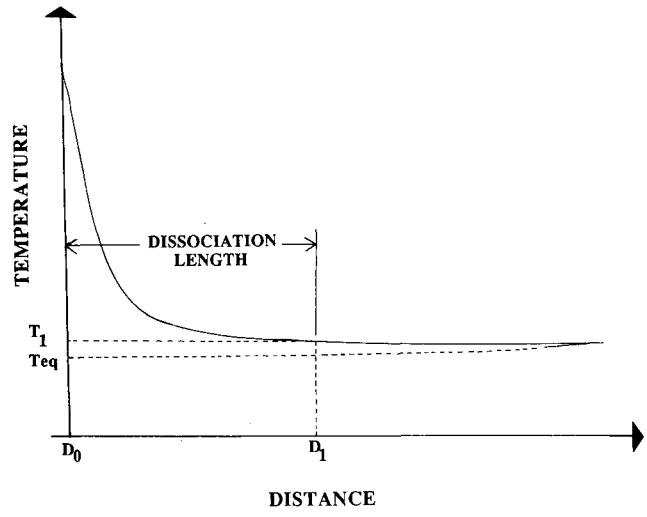

Fig. 3 Temperature relaxation downstream of a shock wave.

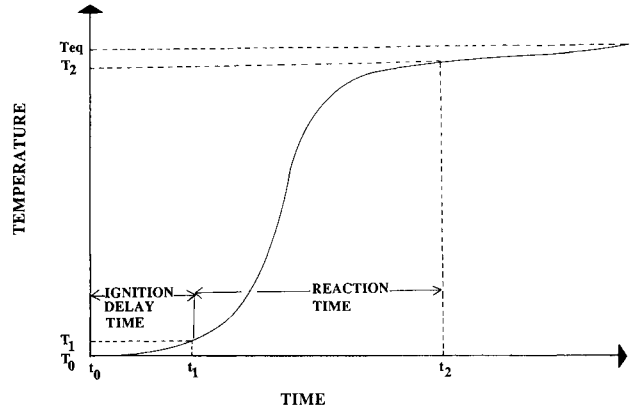

Fig. 4 Temperature relaxation in a combustion process.

The nonequilibrium time and length scales shown in this paper should be viewed as approximate, say within a factor of 2 or so, since for some of the calculations the end points are not well defined. However, every measure has been taken to ensure that the calculations were run to at least 99% of equilibrium. Note that if the cutoffs are chosen to be 99 instead of 95%, the length and time scales increase by approximately 10–50%. Choosing 90% as the cutoff point results in decreasing the length and time scales by approximately 10–50%. Also, since coupled vibration-dissociation, which has been neglected, can substantially increase the relaxation lengths, the error band is large.

Thermal Nonequilibrium

Thermal nonequilibrium occurs when vibrational, rotational, translational, or electronic modes of energy are not in equilibrium. Each is described by a corresponding temperature, which is introduced as a convenient variable to measure energy. Translational temperature is the one we typically measure in gas dynamics. The rotational energy equilibrates with translational energy within a few molecular collisions, and since the mean free path is small throughout the trajectories of interest, the rotational modes of energy are assumed to be in equilibrium with the translational modes. The vibrational and electron energies, however, do not equilibrate as quickly and may be out of equilibrium.

The electron energies will not deviate much from equilibrium for many of the conditions presented here. However, some of the more severe cases (high altitude, high Mach

number) may experience an electron temperature considerably different from the translational temperature. This electron temperature controls radiative phenomena and should be considered in a complete analysis. Here we have chosen to neglect radiation and assume that the electron energies are in equilibrium.

Vibrational nonequilibrium, on the other hand, is important throughout much of the flight corridor. The purpose of this section of the study is to determine the length scales associated with vibrational energy relaxation. In this case, equilibrium simply implies that the vibrational temperature and the translational temperature are equal. Figure 2 shows the variation of temperature through a shock wave with vibrational nonequilibrium.

The vibrational collision mechanism used in this study is N_2 vibrational energy, with N_2 as a collision partner. Since this species is the dominant one and the frequency of collision with N_2 is the greatest, it is believed that this collision process is adequate to estimate the vibrational energy relaxation length. Also, data for this collision mechanism are the most abundant. Other excitation rates are not included and may indicate length scales longer than these estimates. For example, at the higher velocity points in the trajectory, electron-impact vibrational excitation may be important. Also, O_2 and NO vibrational energy were calculated with N_2 and NO as collision partners, respectively, but lengths are typically an order-of-magnitude shorter for the O_2 and two orders-of-magnitude for the NO vibrational energy relaxation. Including additional rates is beyond the scope of this paper.

Order-of-magnitude estimates are obtained from a simple rate model for vibrational nonequilibrium.[23,24] Many different rate models exist, but most are complicated and require constants and parameters that are difficult to determine. Inaccuracies in these experimentally determined parameters make them no better than simplified, curve-fit models for ballpark estimates. The simplest model is a reduced form of the Landau-Teller relationship which, for a steady, inviscid gas, is given by

$$\frac{d}{dx}(ue_v) = \frac{e_v^* - e_v}{\tau(T,p)}$$

where

$$\tau(T,p) = C\frac{e\left(\frac{K}{T}\right)^{1/3}}{p}$$

and e_v^* is e_v evaluated at the translational temperature T, i.e., the equilibrium value. The relaxation parameter τ represents the time it takes to reach the peak vibrational temperature. Vincenti and Kruger[24] have taken Blackman's data[28] and have fitted the following constants for the temperature range 800–6,000 K:

Species: N_2
Partner: N_2
c,atm-μs: 7.12×10^{-3}
K,°K: 1.91×10^6

Multiplying the relaxation time τ by a velocity $u\tau$ gives a characteristic length of the vibrational relaxation process. In this case, u is the velocity after the shock, which is defined as

$$u = \sqrt{V_t^2 + V_{n2}^2}$$

where V_t is the tangengial velocity and is defined by $V_t = V_\infty \sin\theta$. Expression V_{n2} is the normal velocity after the shock and is defined by

$$V_{n2} = V_n \frac{\rho_2}{\rho_\infty}$$

The temperature, pressure, and density T, p, and ρ behind the shock are from the equilibrium air solution results. The vibrational length scales, therefore, assume local chemical equilibrium. Ideally, coupling vibration with dissociation is required, since vibrational relaxation will follow chemical relaxation through the changes in translational temperature. However, since only ballpark estimates are of interest, this simplification was deemed adequate. Note that peak temperature could be used in place of equilibrium temperature. This was not attempted here.

Results

Equilibrium Air

The equilibrium air calculations are performed to study the chemistry behind shock waves characteristic of a hypervelocity vehicle. Since the highest temperatures due to shock heating are from stronger shocks, shock angles of 60 and 30 deg are investigated.

Simple one-dimensional shock relations are used, and it is assumed that the shock wave is infinitesimally thin. The conditions upstream of the shock are the upper and lower trajectory points in Table 1 and are found from the standard atmosphere tables.[10] The velocity used is the normal component of the velocity vector, i.e., $V_n = V_\infty \sin\theta$. Simple assumptions are used in calculating the shock jump conditions. The primary assumption is that the pressure and static enthalpy jumps are insensitive to the composition of the gas. Therefore, ideal-gas jump conditions are used to determine p and h. The shock jump relations used are

$$p = \frac{2\gamma}{\gamma+1}\left(\frac{V_n}{c_\infty}\right)^2 p_\infty$$

$$h = \frac{1}{2}V_n^2[1-\varepsilon^2] + h_\infty$$

where ε is the approximate velocity or density jump and takes on a value of approximately $\frac{1}{6}$ for an ideal gas. From this expression, a density jump only 50% greater contributes a 1.5% error in the expression for enthalpy, which validates the assumption.

The pressure-enthalpy form of the Gordon and McBride algorithm is used with temperature as a variable. The temperature is allowed to vary as energy is absorbed in chemical energy. The output temperature, therefore, is correct for the shock jump, including chemical effects.

The JANAF table used in this study is from Ref. 20 and is valid for two temperature ranges, 1000–6000 K and 6000–15,000 K. The species included are N_2, O_2, N, O, NO, AR, N^+, N_2^+, O^+, O^-, O_2^+, O_2^-, NO^+, AR^+, and e^-. Not all of these species are actually found in any significant quantity, and there are trace species, such as CO_2 and O_3, that are not included. The purpose is to find the major components of the gas, so trace species are considered unimportant. However, if one is interested in the concentrations of the trace species, another study would be required to determine them.

The output is plotted in molar fractions from 10^{-6} to 1.0. Figure 5 shows the equilibrium species concentrations behind a 60-deg shock at points along the trajectory. The abscissa is the Mach number which, when used in conjunction with Table 1, identifies the trajectory point. Calculations are shown at Mach number intervals of 2.5. The 60-deg shock case shows formation of NO as low as Mach 2.5, with peak NO production at Mach 10–12.5. Oxygen begins to dissociate at Mach 5 and nitrogen at Mach 7.5. Monotonic oxygen and nitrogen are present in significant quantities by Mach 15. Ionization first occurs with NO as early as Mach 12.5. This is in agreement with the Wray model for chemical reactions,[23] which suggests that NO^+ is the primary ionized species. Monotonic oxygen begins to ionize at higher Mach numbers.

The 30-deg shock (Fig. 6) has very little dissociation until high Mach numbers and significant ionization, only at the highest Mach number.

Weaker shock waves delay the dissociation to higher Mach numbers. For example, a typical inlet consists of a series of ramps, each of which generates an oblique shock. A series of shocks are used rather than one strong shock so that the total pressure loss behind these shocks is minimized. A consequence of this is that the chemical and vibrational relaxation lengths are long, while the deviation from freestream composition is small. Weak shocks, therefore, indicate little important chemistry and so are not considered in this study.

Normal shocks are not considered here because they are only found at the stagnation point, which is typically nonequilibrium. However, the equilibrium composition behind a 90-deg shock can be found in Ref. 18.

Air Chemical Length Scales

A variety of air chemistry calculations is performed for chemical nonequilibrium flow downstream of shock waves. The shock wave characteristics are chosen to represent typical points on the upper and lower bound SSTOHFAHV trajectory tabulated in Table 1. In addition, two different nonequilibrium air reaction mechanisms are used in an attempt to remove some of the uncertainty associated with the various chemistry models. The air models include a model originally developed by Wray[23] and a second model assembled by Dunn and Kang,[25] which are discussed in Ref. 18. The results from both models are included in the data presented here.

Calculations are preformed for 60- and 30-deg oblique shocks. Figure 7 shows the computed 60-deg oblique shock nonequilibrium length scales for temperature using the two air reaction mechanisms. Length scales for oxygen and nitrogen can be found in Ref. 18. The length scales are shorter on the lower trajectory than on the upper, as is expected with a higher-density gas. The longest relaxation lengths on the lower trajectory are at the lowest Mach number considered, i.e., approximately 300 cm at $M = 10$. The lengths become shorter at higher Mach numbers, i.e., 1 cm at $M = 22.5$. The upper trajectory exhibits different behavior in that the maximum relaxation length, approximately 300 cm, occurs at Mach 25 while the minimum length, approximately 20 cm, occurs between Mach 12.5 and 22.5. Thus, it can be seen that the minimum relaxation length for the upper trajectory is approximately an order of magnitude larger than the lower trajectory. The temperature, oxygen, and nitrogen relaxation lengths typically are within a factor of 2 of each other. Similarly, the Dunn/Kang predictions typically are twice as long as the Wray predictions. Note that both models predict the same peak and equilibrium values. The observed differences in the relaxation lengths predicted by the two models can be attributed to their respective behaviors as each approaches equilibrium. The relaxation history predicted for the Dunn/Kang model tends to flatten out near equilibrium and thus produces a longer relaxation length compared to the Wray model. Over the flight conditions of interest, both models perform well from an engineering standpoint, with the Wray model being the most computationally efficient.

Figure 8 shows the 30-deg shock results. In this case, the longest length scale on the upper trajectory, approximately 800 cm, is found to occur at Mach 17.5, while the shortest length, approximately 300 cm, occurs at Mach 25. For the lower trajectory, the maximum length is approximately 1000 cm at Mach 25, and the shortest length, approximately

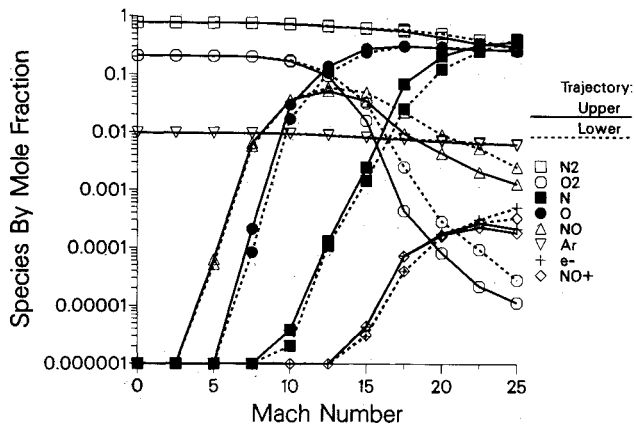

Fig. 5 Equilibrium species distribution behind a 60-deg shock wave.

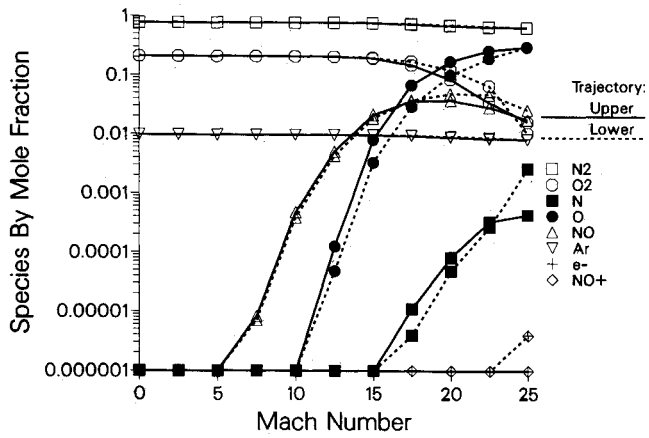

Fig. 6 Equilibrium species distribution behind a 30-deg shock wave.

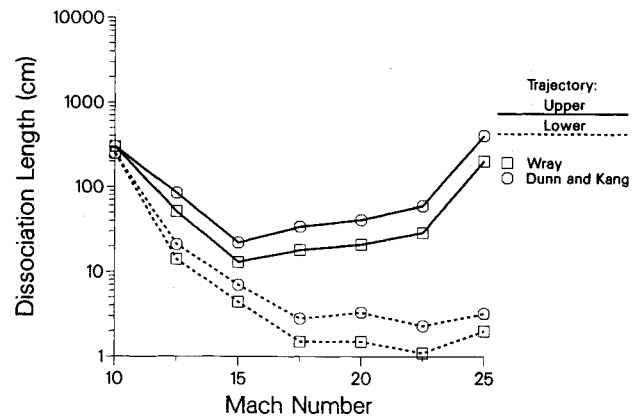

Fig. 7 Nonequilibrium length scales behind a 60-deg shock wave.

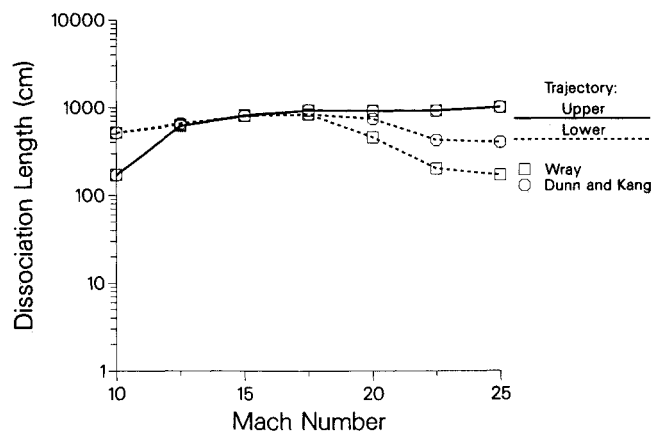

Fig. 8 Nonequilibrium length scales behind a 30-deg shock wave.

500 cm, is found at Mach 10. From the two shock angles considered, it can be seen that the 30-deg shock nonequilibrium relaxation lengths are approximately five times longer than the 60-deg lengths. It should be noted that each point on the figures represents a separate nonequilibrium chemistry calculation.

Air Thermal Length Scales

The N_2-N_2 vibrational length scales are plotted in Fig. 9 for a 90-, 60- and 30-deg shock. The computed length scales use the equilibrium temperature as the translational temperature for e_v^*. In this study, the length scales for vibration are up to several orders of magnitude less than the chemical length scales, indicating that for many cases, chemical nonequilibrium exists but thermal nonequilibrium does not. Note, however, that the thermal length scales are measured as time to peak temperature, whereas the corresponding chemical length scale is measured to 95% of the equilibrium value. Thus, the difference between chemical and thermal length scales is actually less than indicated by this analysis. This suggests that under certain conditions, coupled vibration-dissociation models should be used for a more complete analysis.

Experimental normal shock data from Wray[23] is used to provide a comparison for the computed length scales. These experiments were run at approximately Mach 10, 15, and 20. However, only for the Mach 20 case does the specific pressure and temperature correspond to a trajectory point of Table 1. The experimental data for N_2 vibrational relaxation for this case is marked in Fig. 9 and shows very good agreement with the estimates of this study. Wray's data, in the form of time, is multiplied by the shock speed to get a distance. Appropriate times are determined from the plots in Ref. 23.

Hydrogen-Air Equilibrium

The chemistry associated with the combustor and nozzle is important in determining engine performance. The conditions used to represent this part of the analysis are combustor operating conditions. In this case, no shock waves are present, and it is assumed that the outflow is of a uniform composition. The vital parameters used to characterize the hydrogen-air system at the combustor inflow are the pressure, the temperature, and the fuel equivalence ratio. The fuel equivalence ratio, or ϕ, is defined such that $\phi = 1$ is a stoichiometric mixture of hydrogen and oxygen.

The Gordon and McBride algorithm is used again in this analysis. The JANAF tables used for this section are from Ref. 19, which includes the species associated with H_2-air combustion. Figures 10 and 11 show the equilibrium species concentrations of H_2O and OH for $\phi = 1$ and 6, respectively. Each figure includes pressure of 0.1, 1.0, and 5.0 atm. From these results it is clear that dissociation of the combustion products becomes critical at lower temperatures if the pressure is lowered. For pressures of 1.0 and 5.0 atm, dissociation does not become important until temperatures over 4000 K are reached. For a pressure of 0.1 atm, significant dissociation occurs as low as 3000 K. This result indicates that a constant temperature expansion in the nozzle could hurt engine efficiency. All three plots show similar trends, which indicates that the equilibrium values are not strongly dependent on equivalence ratios. However, the benefit of cooling from the added fuel has not been taken into account in this analysis.

Reference 18 gives equilibrium species concentrations for some of the dissociation products for $\phi = 1$, $p = 1$ atm. Species H and O account for much of the energy absorption. At the highest temperatures, other species become important.

Hydrogen-Air Time Scales

A series of H_2-air nonequilibrium calculations are performed using the CHEMKIN code along with the H_2-air reaction mechanism developed by Jachimowski.[27] The mechanism is described in Ref. 18 and is considered valid over the temperature and pressure ranges considered in this article. The calculated results presented here are intended to represent reaction time scales for a series of temperatures and pressures typical of scramjet combustors. Pressures from 0.1–5 atm, temperatures from 1000–3000 K, and ϕ from 1–6 are considered in this article.

The results of these calculations are summarized in Figs. 12–17. Figures 12 and 13 represent the reaction time scales for temperature and H_2O production for $\phi = 1$. Similarly, Figs. 14 and 15 represent the $\phi = 3$ results and Figs. 16 and 17 the $\phi = 6$ results. All three ϕ cases show that the time scales associated with temperature and H_2O relaxation decrease with

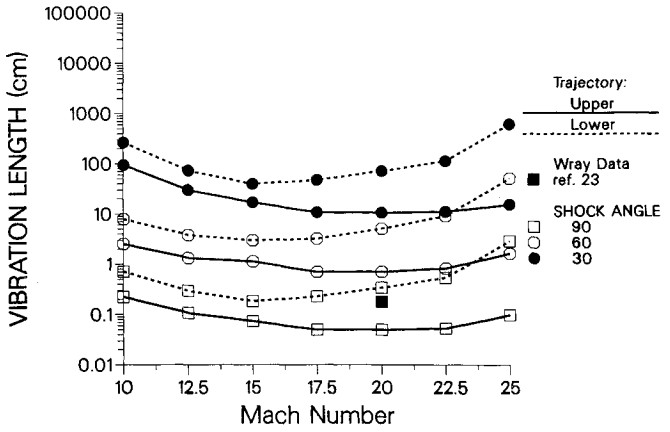

Fig. 9 Thermal nonequilibrium length scales.

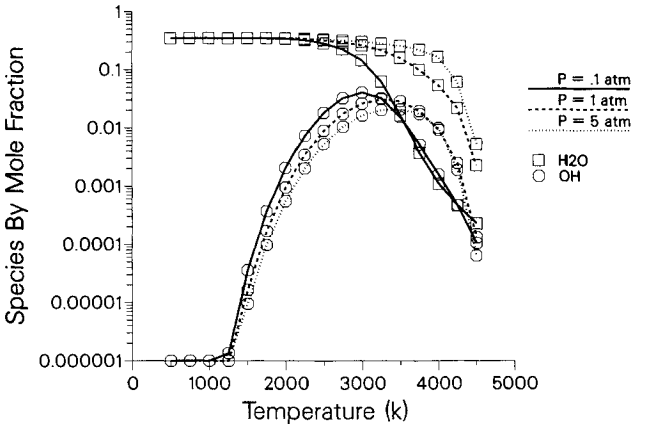

Fig. 10 Equilibrium species distribution for H_2-air combustion, $\phi = 1$.

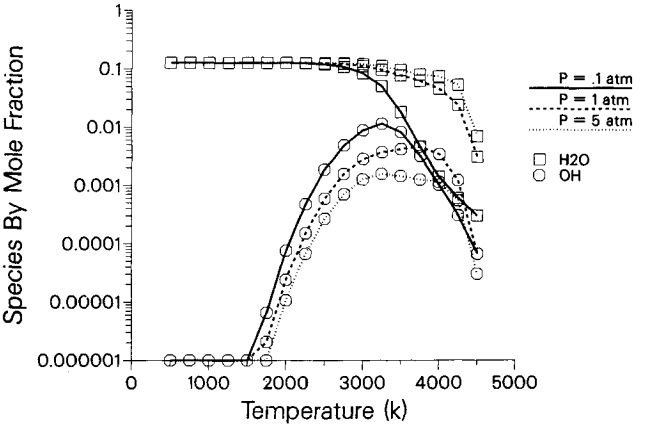

Fig. 11 Equilibrium species distribution for H_2-air combustion, $\phi = 6$.

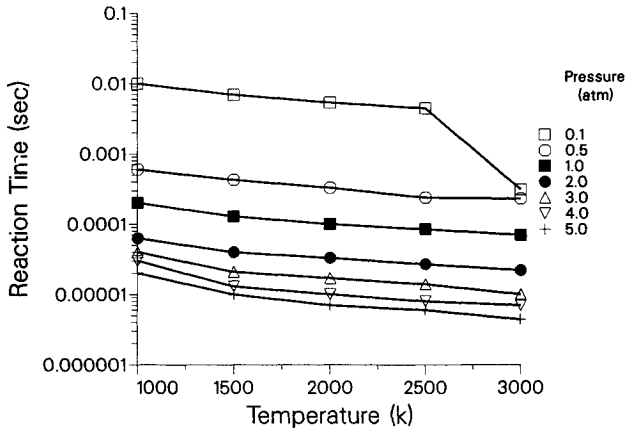

Fig. 12 Temperature relaxation for H_2-air combustion, $\phi = 1$.

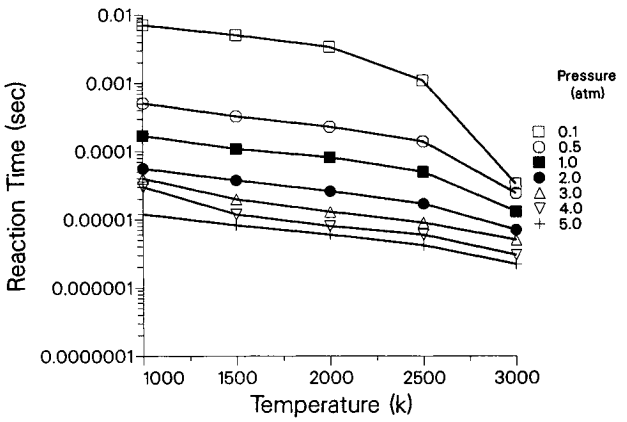

Fig. 13 H_2O relaxation for H_2-air combustion, $\phi = 1$.

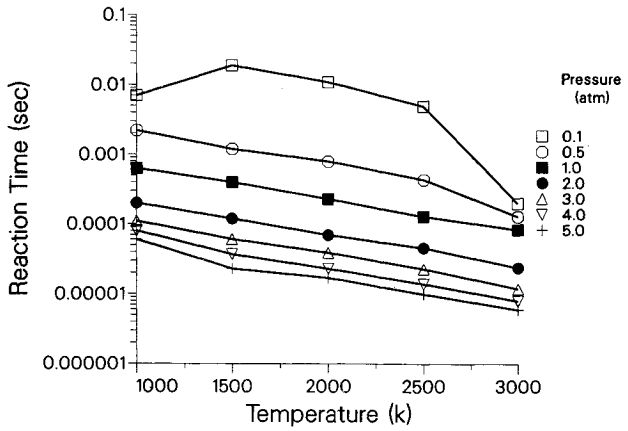

Fig. 14 Temperature relaxation for H_2-air combustion, $\phi = 3$.

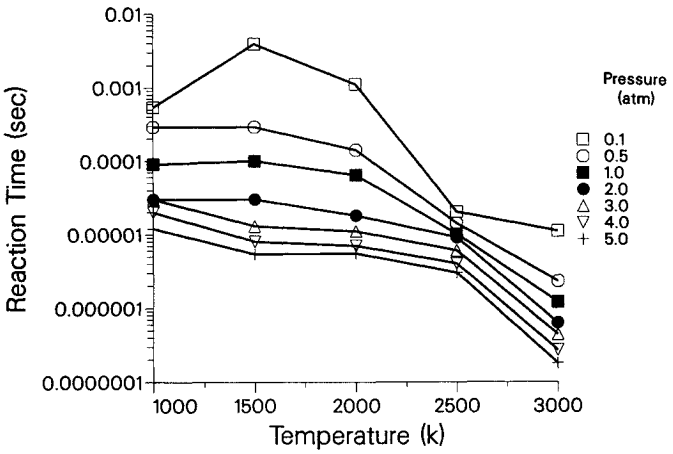

Fig. 15 H_2O relaxation for H_2-air combustion, $\phi = 3$.

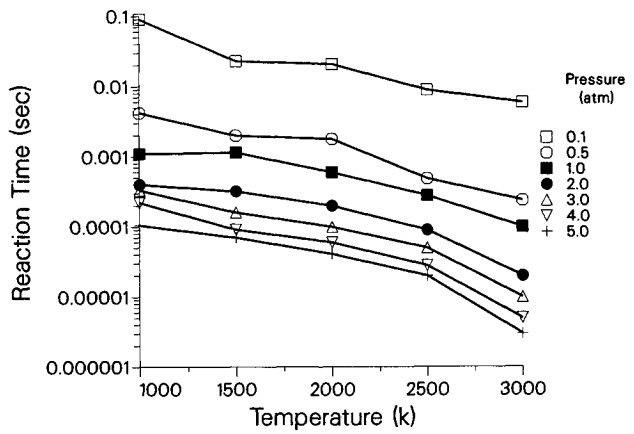

Fig. 16 Temperature relaxation for H_2-air combustion, $\phi = 6$.

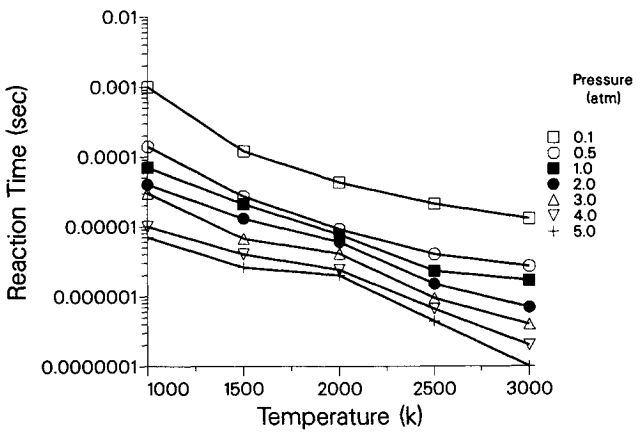

Fig. 17 H_2O relaxation for H_2-air combustion, $\phi = 6$.

increasing temperature and pressure. For the cases run with $\phi = 1$, the time scale for temperature relaxation ranges from 10^{-5} s ($p = 5$ atm, $T = 3000$ K) to 10^{-2} s ($p = 0.1$ atm, $T = 1000$ K). A similar behavior is found for the H_2O relaxation time scales. Typically, the H_2O relaxation times are 10–50% shorter than the temperature relaxation times. Comparing the relaxation times for the various ϕ shows that the temperature relaxation times for a ϕ of 6 are approximately 10 times longer than for a ϕ of 1. The H_2O relaxation times are found to exhibit the opposite behavior. In particular, the H_2O relaxation times for a ϕ of 6 are approximately 1/10 that for a ϕ of 1. Finally, the reaction length scales can be computed by multiplying the reaction time by the local fluid velocity. For example, typical velocities in the combustor range from 300,000–700,000 cm/s, which for $\phi = 1$, $p = 0.5$ atm, and $T = 1500$ K translates to reaction lengths between 150 and 350 cm.

Conclusions

A generic SSTOHFAHV and its trajectory have been studied to determine the level of chemical modeling required for computational design codes. In particular, the air chemistry

associated with a hypersonic vehicle forebody and the H_2-air chemistry associated with the combustor and nozzle have been studied. Important conclusions about the chemical properties of each of these regions can be drawn from the results.

The length scales associated with air dissociation on a hypersonic vehicle forebody were found to have a strong dependence on the trajectory. The lower and upper bounds of the SSTOHFAHV trajectory show large differences in relaxation lengths. The lower trajectory, due to the higher density of the air, can be modeled mostly with chemical equilibrium, except at the highest Mach numbers. The upper trajectory, on the other hand, has length scales that indicate the importance of nonequilibrium chemistry. Therefore, either equilibrium or nonequilibrium chemical modeling will be required, depending on the trajectory. The 60-deg shock produces relatively short relaxation lengths, while the 30-deg shock produces relatively long relaxation lengths.

The H_2-air chemistry inside a scramjet combustor and nozzle can be characterized in a number of ways. In this paper an attempt has been made to consider the effect of pressure, temperature, and ϕ on combustion time scales. For all the cases considered, it was found that increasing the static temperature and pressure reduced the reaction times significantly. Pressure has the most notable effect as a consequence of the particular reaction scheme used in this paper. The scheme tends to generate equilibrium coefficients that are strongly dependent on pressure. For example, with a ϕ of 1, the time scales decreased by approximately three orders of magnitude when the pressure was increased from 0.1 to 5 atm. Similar trends were noted for the higher ϕ. Increasing ϕ caused the temperature nonequilibrium time scale to increase but the H_2O time scales to decrease. The equilibrium calculations showed that the temperature at which H_2O began to dissociate was strongly dependent on static pressure. In particular, the lower the static pressure, the lower the static temperature required for H_2O to begin dissociating. This would suggest the upper limit on both pressure and temperature to maximize H_2O or heat release in the combustion process.

Acknowledgments

The authors would like to thank Drs. Kee and Mitchell of Sandia for providing the CHEMKIN programs and Dr. Jachimowski of NASA Langley for providing the H_2-air chemistry mechanism.

References

[1]Howe, J. T., "Introductory Aerothermodynamics of Advanced Space Transportation Systems," *Journal of Spacecraft and Rockets*, Vol. 22, Jan.–Feb. 1985, pp. 19–26.

[2]"Propelling the Aerospace Plane," *Mechanical Engineering*, June 1986, p. 32.

[3]Eberhardt, D. S. and Brown, K. G., "A Shock Capturing Technique for Hypersonic, Chemically Relaxing Flows," AIAA Paper 86-0231, Jan. 1986.

[4]Park, C., "On Convergence of Computation of Chemically Reacting Flows," AIAA Paper 85-0247, Jan. 1985.

[5]Carofano, G. C., "Blast Computation Using Harten's Total Variation Diminishing Scheme," U.S. Army ARDC, ARLCB-TR-84029, Oct. 1984.

[6]Bussing, T. R. A. and Murman, E. M., "A Finite Volume Method for the Calculation of Compressible Chemically Reacting Flows," AIAA Paper 85-0331, Jan. 1985.

[7]Tannehill, J. C. and Mugge, P. H., "Improved Curve Fits for the Thermodynamic Properties of Equilibrium Air Suitable for Numerical Computation using Time-Dependent or Shock-Capturing Methods," NASA CR-2470, 1974.

[8]Bray, K. N. C., "Real Gas Effects on Lifting Re-Entry Aerothermodynamics," *Aerodynamic Problems of Hypersonic Vehicles*, AGARD-LS-42, Vol. 1, July 1972.

[9]Couch, L. M., Calspan-UB Research Center Short Course in Hypersonics, State Univ. of New York at Buffalo, Buffalo, NY, Aug. 19–22, 1986.

[10]U.S. Standard Atmosphere, 1962.

[11]Tauber, M. E., Menees, G. P., and Adelman, H. G., "Aerothermodynamics of Transatmospheric Vehicles," AIAA Paper 86-1257, 1986.

[12]Gordon, S. and McBride, B. J., "Computer Program for Calculation of Complex Chemical Equilibrium Composition, Rocket Performance, Incident and Reflected Shocks, and Chapman-Jouguet Detonations," NASA SP-273 (Interim Revision), 1976.

[13]White, W. B., Johnson, S. M., and Dantzig, G. B., "Chemical Equilibrium in Complex Mixtures," *Journal of Chemical Physics*, Vol. 28, May 1958, pp. 751–755.

[14]Green, M. J. and Davy, W. C., "CAG12—A CSCM Based Procedure For Flow of an Equilibrium Chemically Reacting Gas," AIAA Paper 85-0927, June 1985.

[15]Eberhardt, D. S. and Palmer, G., "A Two-Dimensional, TVD Numerical Scheme for Inviscid, High Mach Number Flows in Chemical Equilibrium," AIAA Paper 86-1284, June 1986.

[16]Davy, W. C., Lombard, C. K., and Green, M. J., "Forebody and Base Region in Severe Planetary Entry by a Factored Implicit Numerical Scheme," AIAA Paper 81-0282, Jan. 1981.

[17]Moss, J. N., "Radiative Viscous-Shock-Layer Solutions with Coupled Ablation Injection," *AIAA Journal*, Vol. 14, Sept. 1976, pp. 1311–1317.

[18]Bussing, T. R. A. and Eberhardt, D. S., "Chemistry Associated with Hypersonic Vehicles," AIAA Paper 87-1292, June 1987.

[19]Stull, D. R. and Prophet, H., "JANAF Thermochemical Tables, 2nd ed.," NSRDS Rept. 37, National Bureau of Standards, June 1971. (Also updates supplied by Dow Chemical Company, DE.)

[20]Esch, D. D., Siripong, A., and Pike, R. W., "A Technical Report on Thermodynamic Properties in Polynomial Form For Carbon, Hydrogen, Nitrogen, and Oxygen Systems from 300 to 15000°K," NASA-RFL-TR-70-3, Nov. 1970.

[21]Kee, R. J., Miller, J. A., and Jefferson, T. H., "CHEMKIN: A General-Purpose, Problem-Independent, Transportable, Fortran Chemical Kinetics Code Package," Sandia Rept. SAND80-8003, March 1980.

[22]Mitchell, R. E. and Kee, R. E., "A General-Purpose Computer Code for Predicting Chemical Kinetic Behavior Behind Incident and Reflected Shocks," Sandia Rept. SAND82-8205, March 1982.

[23]Wray, K. L., "Chemical Kinetics of High Temperature Air," ARS International Hypersonics Conference, Cambridge, MA, Aug. 16–18, 1961.

[24]Vincenti, W. G. and Kruger, C. H., *Introduction to Physical Gas Dynamics*, Krieger, Malabar, FL, 1965, pp. 222–232.

[25]Dunn, M. G. and Kang, S. W., "Theoretical and Experimental Studies of Reentry Plasmas," NASA CR-2232, April 1973.

[26]Park, C., personal communications, June 1987, and "Two-Temperature Interpretation of Dissociation Rate Data," AIAA Paper 88-0458, Jan. 1988.

[27]Jachimowski, C., private communications, April 1987.

[28]Blackman, V., "Vibrational Relaxation in Oxygen and Nitrogen," *Journal of Fluid Mechanics*, Vol. 1, Part I, 1956, pp. 61–85.